Heliyon 10 (2024) e31823

Contents lists available at ScienceDirect

Heliyon

journal homepage: www.cell.com/heliyon

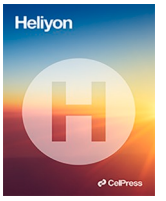

Research article

Sustainable production of porous chitosan microparticles by energy-efficient membrane emulsification

Suchintan Mondal [1], Márcia T. Tavares [1], Carla Brazinha [*]

LAQV/Requimte, Department of Chemistry, NOVA School of Science and Technology, FCT NOVA, Universidade NOVA de Lisboa, 2829-516, Caparica, Portugal

ARTICLE INFO

Keywords:
Chitosan microparticles
Direct membrane emulsification
Porous particles
Drug capture
Drug release

ABSTRACT

In drug delivery, it is common to use porous particles as carrier media, instead of dense particles, due to their high specific surface area and available entrapment volume, which allows a higher amount of drug to be encapsulated and then released. Chitosan microparticles are extensively used in drug delivery, but porous chitosan microparticles are scarcely reported. In this work, the preparation of porous chitosan microparticles using membrane emulsification is addressed, a technology that involves mild operating conditions and less energy consumption than traditional methods (such as ultrasound), and with higher control of the particle size. The dense structure is obtained by a water-in-oil emulsion. The porous structure is obtained by a gas-in-water-in-oil G/W/O double emulsion, where argon bubbles get entrapped in an aqueous chitosan solution that is further emulsified in a paraffin/petroleum ether mixture. Porous chitosan particles were obtained with sizes of 7.7 ± 1.6 μm, which was comparable with dense chitosan particles (6.2 ± 2.3 μm). The pore structure was optimized by varying the argon flow rate, being optimized at 0.24 L h^{-1}. The impact of drug loading by adsorption or encapsulation, and of the drug release behaviour when using porous and dense particles were assessed, using the protein bovine serum albumin (BSA) as a model drug. The results showed that by encapsulating BSA the loading efficiency was above 95 % for both types of particles, with the release being slightly slower for the dense particles. As for the adsorbed BSA, the loading efficiency was significantly higher for porous particles – 70 % - against the 40 % for dense particles. Porous chitosan particles were successfully obtained using the membrane emulsification technology and showed that these carriers are advantageous regarding drug loading and release.

1. Introduction

In modern healthcare research, one of the prudent quests is to improve drug delivery systems. Among the multi-facet challenges encountered, one of the critical aspects is to encapsulate the drug of interest in the particle in a way that its bioactivity is retained, and its bioavailability improves [1]. In order to maximise the amount of encapsulated drug, some of the critical aspects are the size and morphology of the particles. For example, microporous particles possess an advantage due to their porous morphology and smaller size that leads to higher specific surface area [2]. Chitosan is an accessible, natural, biodegradable and biocompatible material that shows

* Corresponding author.
E-mail address: c.brazinha@fct.unl.pt (C. Brazinha).
[1] Equal contributing authors.

https://doi.org/10.1016/j.heliyon.2024.e31823
Received 27 November 2023; Received in revised form 1 April 2024; Accepted 22 May 2024
Available online 23 May 2024

mucoadhesive properties which make it ideal for drug delivery applications [3]. In fact, chitosan particles have been extensively studied in this field and can be synthesised by using different methodologies. A very common way to obtain chitosan particles is by ionic gelation using sodium tripolyphosphate (TPP) as an anionic crosslinking agent [4]. Particles can also be obtained by solvent evaporation or precipitation [5]. However, in these techniques, control over the particle size and uniformity is more difficult, which limits the reproducibility of the processes [6].

Membrane emulsification is an energy-efficient emulsification technique where the formation of the droplets is largely dependent on pore size and pore size distribution of the membrane. Also, other factors contributing to the droplet formation: hydrophilicity/hydrophobicity of the active layer of the membrane (layer where the droplet is built), shear stress of the continuous phase on the active layer of the membrane, *trans*-membrane pressure and interfacial tension between the two phases of the emulsion [7]. It is a greener process that applies low mechanical stress, consumes less energy and shows reproducibility, while controlling the size of the droplets in a more efficient manner than emulsions formed by traditional methods like ultrasonic waves, high-speed stirring etc. [1,8] However, scaling up of the process for industrial production is one of the challenges along with availability of wide range of membranes fit for the process. There are some works in the literature where nano- or micro-sized particles of chitosan were obtained by membrane emulsification, using mostly Shirasu Porous Glass (SPG) membranes [6]. To obtain these particles, techniques such as the premix emulsification and the rotating cell dispersion were used [9,10]. However, while the premix emulsification requires several cycles to obtain the particles with the ideal size, the rotating cell is much harder to scale up. Besides, to the best of our knowledge, there are no reports of porous chitosan particles obtained by direct membrane emulsification, and the known porous chitosan particles were either capsules obtained by using templates, or they are mixed with other polymers [11–13]. As described by Wang et al. porous chitosan particles can be produced by using specific structured templates in between the chains of the chitosan polymer and then subsequently the templates are removed [11,12,14,15]. However, when using templates, it is not possible to load drugs during the synthesis step, they could only be adsorbed once the templates are removed. Besides, the templates need to be synthesised themselves, and the removing technique can be time-consuming and often requires further usage of organic solvents and surfactants [11].

By applying ultrasound waves through acoustic cavitation to a polymeric solution containing a surfactant it is also possible to form air bubbles that will stay stabilized until the polymerization step [16]. However, by using this technique it is not possible to control the size of the air bubbles and the size and polydispersity of the particles [17]. Other techniques such as chemical reactions, coaxial electrohydrodynamic atomisation technique or microfluidics are also used to prepare such particles [18–22]. In microfluidics, even though it is possible to control the size and morphology, the production rate is very low, and it is not scalable [18]. All these techniques also have the disadvantage of using more than one solvent in order to obtain the porous particles. In green chemistry, an effort must be made to minimise the use of organic solvents that can negatively affect the environment. Even though it is still not possible to completely avoid the use of these solvents, by using a gas to form the pore structure of the particles there is a chance to skip a step of synthesis or chemical reaction, which contributes to the greening of the process [23].

Other techniques were applied where bubbles functioned as templates for the production of hollow particles, which has been demonstrated to be useful in energy storage and extraction [21,24]. There are reports on the use of membrane emulsification technique to obtain gas bubbles in liquid solutions (G/W) using nitrogen, or perfluorocarbon as gas sources [25–27]. Chen et al. used Janus membrane emulsification, where one side of the membrane is hydrophilic and the other is hydrophobic, to obtain hollow spheres by performing a G/O/W double emulsion [28]. However, this is the only report of the production of hollow particles using membrane emulsification, and no reports were found regarding the production of porous particles.

In this work, our goal was to obtain porous chitosan microparticles by the production of a G/W/O double emulsion using the direct membrane emulsification technique. The novelty relies mainly on the production of porous particles using this technique. The loading of a model drug (BSA) on the particles was also investigated both by incorporating it inside the polymeric matrix and by adsorbing it on the particle surface. Furthermore, by comparing porous and dense particles, it will be possible to show the effects of the porosity on the loading and release profile of the model drug.

2. Materials and methods

2.1. Materials

Nucleopore track-etch membranes (Polycarbonate, 0.08 μm nominal pore size, 25 μm thickness) were purchased from Whatman™, USA. Metallic isoporous membranes, fabricated by our group, with active surface pores of 9 μm were obtained by laser machining, as previously described [29]. In order to make the membranes hydrophobic in one of the sides, an active layer is obtained by silylation on the side with 9 μm pores [30]. The hydrophobicity is confirmed by measuring the contact angle using a drop shape analyser (Krüss, Germany). Chitosan (CHT, M_w 50,000–190,000), sodium tripolyphosphate (TPP), glutaraldehyde solution (GHT, 25 %), petroleum ether, paraffin oil, acetic acid, Tween® 20, Span® 80, bovine serum albumin (BSA, heat shock fraction, pH 7, ≥98 %) and fluorescein isothiocyanate (FITC) were all purchased from Merck, Portugal. For phosphate buffer solution (PBS, pH 7.4): sodium chloride (NaCl), potassium chloride (KCl), sodium hydrogen phosphate, anhydrous (Na_2HPO_4) and potassium phosphate monobasic (KH_2PO_4) were purchased from Merck, Portugal.

2.2. Experimental setup

A syringe pump (Harvard Apparatus, PHD ULTRA 4400 I/W PROG, USA) is used to inject the dispersed phase through the membrane using a stainless-steel syringe as shown in the schematic diagram of the process in Fig. 1. The flat sheet membrane had an

active surface of 2.9×10^{-4} m^2 and it was enclosed in a plexi-glass emulsification module. The flow rate of the dispersed phase was set in the syringe pump while the continuous phase (aqueous solution of surfactant and biopolymer) was recirculated using a peristaltic pump (Watson Marlow, 530s, UK). The crossflow velocity of the continuous phase is described in equation (1):

$$\nu = \frac{4 * Q_{CP}}{\pi * D_h^2} \quad [1]$$

where Q_{CP} [$m^3 . s^{-1}$] is the continuous phase flow rate and D_h [m] is the hydraulic diameter of the flow channel on the continuous phase at the membrane module. The D_h depends on the cross-sectional area A [m^2] and perimeter of the channel P [m], as described in equation (2).

$$D_h = \frac{4A}{P} \quad [2]$$

2.3. Production of porous chitosan particles

The membrane emulsification methodology was first adapted from the work of Mondal et al. [7] The main parameters involved in this technique were the choice of membranes (track-etch membrane and metallic membrane), composition of dispersed phases and continuous phases, flow rates of dispersed phase and continuous phases, choice of surfactants. The first step to produce the G/W/O double emulsions was to obtain a gas-in-water emulsion, with argon bubbles in a chitosan solution (G/W) (Fig. 1A). An argon stream at different flow rates (0.06 L h^{-1}, 0.24 L h^{-1} or 0.9 L h^{-1}) was injected into a 0.08 μm pore track-etch membrane and a continuous phase of 20 mL of 1.5 % (w/v) chitosan in 2 % (w/v) acetic acid aqueous solution and 5 % (w/v) Tween 20, was being recirculated at a

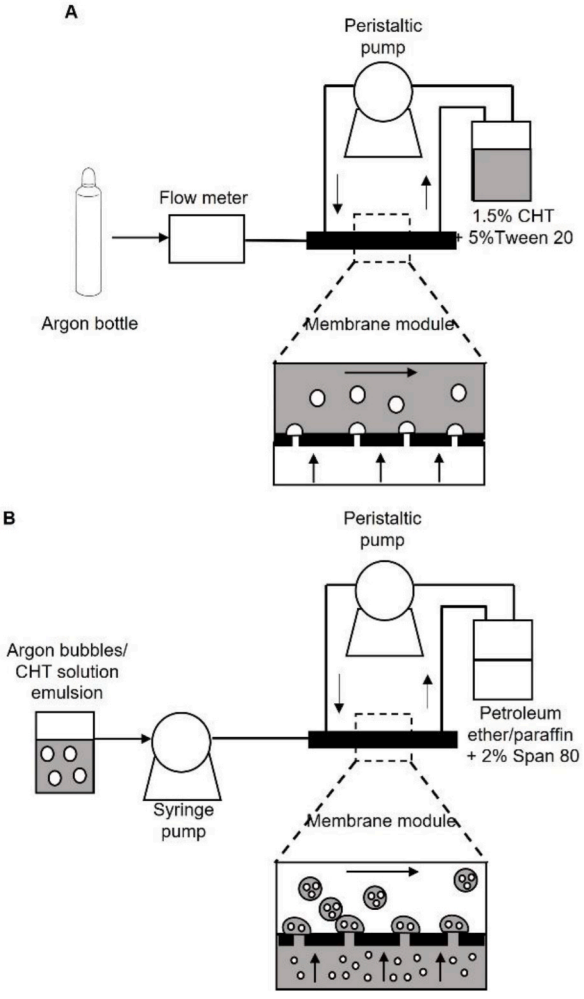

Fig. 1. Experimental setup of the membrane emulsification process to obtain CHT porous particles. (A) Production of G/W emulsion. (B) Production of G/W/O double emulsion.

cross-flow velocity of 0.05 m s^{-1}. Tween 20 was chosen as the surfactant to be added to the aqueous solution because by having a hydrophilic-lipophilic balance (HLB) value of 16.7 it promotes formation of G/W emulsions.

The second step consists of producing the double emulsion (G/W/O) (Fig. 1B) and was adapted from Melich et al. [27] Microbubbles are increasingly used in several fields, such as medical imaging for enhanced contrast ultrasound imaging. Theses microbubbles usually consist of a gas core stabilized by surfactant molecules. Melich et al. conducted a study utilizing Shirasu Porous Glass (SPG) membranes to generate perfluorocarbon microbubbles, focusing on their size, distribution, and stability [27]. They examined various parameters affecting microbubble size, including transmembrane pressure, bubble point pressure, shear stress, membrane pore size, types of gases and surfactants. Interestingly, microbubble size and size distribution were not influenced by either of transmembrane pressure or shear stress, when the ratio of transmembrane pressure to bubble point pressure was less than 1.5. Decreasing membrane pore sizes resulted in smaller microbubbles but increased size distribution due to higher Laplace pressure destabilizing smaller bubbles. Using a 1.1 μm pore sized membrane, perfluorocarbon microbubbles with sizes around 13.3 μm (coefficient of variation (CV) of 16 %), 15.6 μm (CV of 23 %) and 16.5 μm (CV of 26 %) were obtained when stabilized by sodium dodecyl sulphate, Tween 20 and polyoxyethylene (40) stearate respectively. Perfluorocarbon microbubbles were smaller than air microbubbles due to lower surface tension, enhancing their retention at pore openings. Stability tests showed that perfluorocarbon gas prolonged microbubble lifetime compared to air, with minimal increase in size over time. Hence a more effective, controlled and reproducible production of perfluorocarbon microbubbles was achieved by membrane technique. The key factor in microbubble formation was surfactant adsorption kinetics at the gas-liquid interface. Another study investigated microbubble generation using commercial porous filtration membranes in aqueous or organic liquids under a liquid cross-flow [31]. Several ceramic membranes made of alumina or zirconium oxides and having tubular configuration with varying pore sizes (20–800 nm) successfully generated microbubbles. Bimodal distribution (microbubble size distribution measured using "Spraytec" instrument from Malvern Panalytical) of microbubbles were formed in heptane, with different zirconium oxide membranes under varying shear stresses, demonstrating potential for improving gas/liquid mass transfer operations.

In the present work, 2.5 mL of chitosan solution containing the Ar bubbles is now the dispersed phase, being pressurized through the modified stainless steel metallic membrane with an active side consisting of uniform pore size of 9 μm, with a flow rate of 40.4 L h^{-1} m^{-2}. The continuous phase is molar mixture (ratio 5:7) of petroleum ether (PE) and paraffin oil (PO), and 2 % (w/v) Span 80 and circulated at 0.05 m s^{-1}. Span 80 has a HLB value of 4.3, thus being soluble in the oil phase [32]. To obtain dense chitosan microparticles, only the second step is followed (W/O). In order to crosslink the chitosan microparticles, 1 mg mL^{-1} of TPP is added at a rate of 0.012 L h^{-1} and left stirring for an hour at 200 rpm. After, GHT-saturated toluene is added dropwise and left stirring for an hour.

The particles are centrifuged at 1000 rpm using a centrifuge (OHAUS® 5706, USA) and washed three times using petroleum ether and once with water. To completely remove the petroleum ether, they are left to dry overnight at room temperature.

2.4. Production of BSA-loaded chitosan microparticles

The addition of BSA can be done either by incorporation in the particles structure or by adsorption after the synthesis of the particles. In the incorporation methodology, BSA is added to the chitosan solution and the membrane emulsification procedure is applied as mentioned previously. When adsorbed, BSA is added to a dispersion of CHT particles in PBS buffer and left stirring for 1 h. The particles are then centrifuged, and the supernatant is saved to measure the encapsulated BSA.

2.5. Microparticles characterization

The microparticles were characterised using an optical microscope (Nikon H550S, Japan) to do a qualitative evaluation of morphology and aggregation. Confocal laser scanning microscopy (CLSM, Zeiss LSM 880, Germany) was also used to obtain particle size and the pore structure. In order to provide fluorescence to the particles, FITC was added in the chitosan solution and was left stirring for 1 h before proceeding with the membrane emulsification step. The diameter of the particles and pores was obtained by measuring the diameter of n = 50 using ImageJ software [33].

2.6. BSA encapsulation and release

The amount of encapsulated BSA was calculated by quantifying the BSA present in the supernatant after incorporation using UV spectrophotometry. The BSA concentration was obtained by measuring the absorbance at 280 nm using a spectrophotometer (Thermo Scientific evolution 201, Spain) and the encapsulation was calculated as given in equation (3):

$$\%E = \frac{(\textit{total amount of BSA} - \textit{free amount of BSA in supernatant}}{\textit{total amount of BSA}} \text{ x } 100 \quad [3]$$

For the release studies, 5 mL of PBS was added to the centrifuged particles and were placed in an orbital shaker (OHAUS®, USA) at 37°C and 150 rpm agitation. At specified times, 0.5 mL sample was taken from the tube and substituted for 0.5 mL of fresh PBS. The BSA concentration was quantified by measuring the absorbance at 280 nm. All the measures were done in triplicates.

3. Results and discussion

3.1. Preparation of porous chitosan microparticles

In order to obtain a porous structure in the chitosan microparticles, a gas-in-water emulsion (G/W) was prepared using argon as the dispersed phase and chitosan aqueous solution as the continuous phase. For the initial studies, the argon flow rate used was 0.24 L h^{-1}. In Fig. 2A and B we can observe the bubbles of argon stable in the chitosan after 20 and 40 min respectively. The first thing to point out is that after 20 min in solution, the bubbles remain present, and after 40 min there was only a small reduction in their number. In order to stabilise the microbubbles in the chitosan solution, it is important to add a hydrophilic surfactant, in this case Tween20. The Tween20 adsorbs at the gas-liquid interface and reduces the interfacial tension. This avoids coalescence of bubbles and keep them stable for longer. The presence of the surfactant is also responsible for the successful detachment of the bubbles from the membrane [31]. Regarding the size of the bubbles and considering the ones that were possible to measure from the images obtained, the diameter was 3.77 ± 1.33 μm. Due to the resolution limit of the microscope used, nanosized bubbles were not measured.

To obtain the porous particles, a double emulsion was produced, using the previous G/W emulsion as the dispersed phase and solution of paraffin oil, petroleum ether and Span 80 (PO/PE/Span80) as the continuous phase. For the successful detachment of the drops from the membrane, it is important to have a hydrophobic surface on the continuous phase side. The available metallic membranes showed a water contact angle of 70°, so a functionalization step using silanol groups was performed and the contact angle increased to 145° thereby making the surface superhydrophobic. After the emulsion was produced, a crosslinking step was done. Glutaraldehyde (GHT) is the most used crosslinker for chitosan, however it is toxic. Some studies showed that its presence could cause denaturation of proteins, so a two-step crosslinking is applied to prevent effects on the drug's conformation and its release. In the first step, non-toxic tripolyphosphate (TPP) is added to do an ionic gelation step, and then the GHT is added to do a covalent crosslinking [6]. In the ionic gelation there is an ionic interaction between amino groups of chitosan and phosphoric groups of the TPP. When the GHT is added, its aldehyde groups form a covalent bond with the remaining free amino groups of the chitosan, increasing the bonding of the chains in a much smaller concentration than if it was the only crosslinker used.[5] By comparing particles obtained in a single (Fig. 3A) and double emulsion (Fig. 3B) (dense and porous respectively) it is possible to see that the particles maintain their size and morphology after the entrapment of the argon bubbles. Dense particles showed an average diameter of 6.2 ± 2.3 μm while the porous particles showed a 7.7 ± 1.6 μm diameter. The washing step of the particles involves the use of, at a first step, petroleum ether and then water. The petroleum ether is used to take the remaining paraffin oil, while the water will help remove remaining GHT. Also, it is crucial to be able to disperse the particles in water for the loading and release studies. In Fig. 3C it is possible to observe the CHT particles dispersed in water after the washing step. The particles size when in water is 7.9 ± 2.3 μm, remaining comparable to the particles in continuous phase. The washing step did not affect the particles size and they kept disaggregated.

To have images of the particles with higher resolution, confocal microscopy images were obtained. In Fig. 4A we can see a dispersion of porous CHT particles with an improved quality. Using these images, the particle size obtained was 6.7 ± 3.8 μm, which agrees with the sizes obtained by optical microscope. However, the standard deviation is slightly higher due to the presence of bigger particles, with sizes close to 20 μm. Considering that 50 particles are considered, such statistical variations are not unusual. Even using this ampliation, it is possible to observe the pores of the particles, although not in high definition.

By using a higher resolution, it was possible to optimise the bubble formation focusing mostly on their size and dispersity. To have more precise results, the chosen particles to do this study are around 20 μm, which is above the average size. This way we can better observe the bubbles and compare them between assays. Three different argon flow rates were tested: 0.06 L h^{-1} (Figs. 4C), 0.24 L h^{-1} (Fig. 4B) or 0.9 L h^{-1} (Fig. 4D). When using a slower flow rate, the bubbles size is around 2.6 ± 1.9 μm, and the number of bubbles per particle is very low. On the other hand, using a flow rate of 0.9 L h^{-1}, the bubbles size increases to 12 ± 1.8 μm and occupy the majority of the particles volume, forming something similar to a capsule. When using an intermediate flow rate of 0.24 L h^{-1} the mean diameter of bubbles was 6.8 ± 2.9 μm. Because of the specific large particles used to conduct this study, the bubbles diameter cannot be compared with the values obtained by optical microscope. Also, the number of bubbles per particles increase. Although the polydispersity of the bubbles increase, they are better distributed within the particle forming the desired pore structure. Previous studies

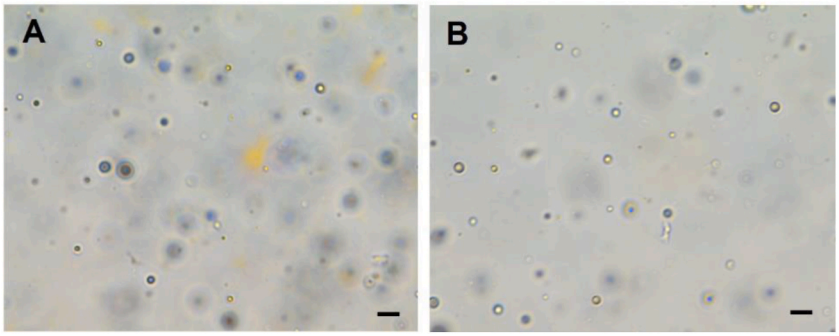

Fig. 2. Optical microscope images of Argon bubbles after 20 (A) and 40 min (B) in the chitosan solution. Scale bar = 10 μm.

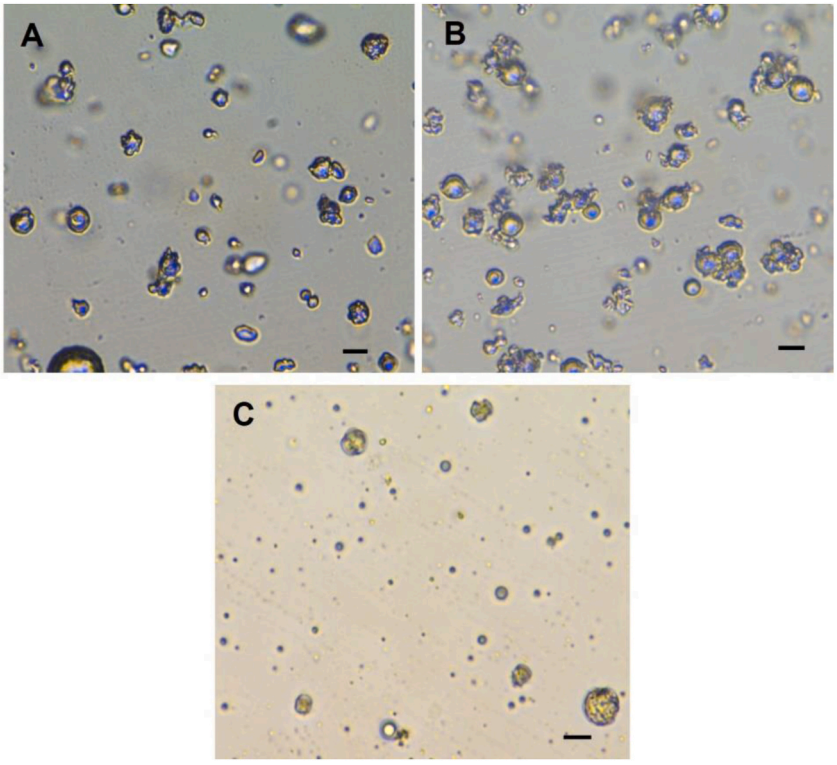

Fig. 3. Optical microscope images of chitosan microparticles. Dense (A) and porous (B) microparticles dispersed in the continuous phase (PO/PE/Span80). Porous particles dispersed in water after washing (C). Scale bar = 10 μm.

that obtained porous particles by the use a gas stream also faced the challenge of not having a monodisperse pore network [34]. During the first step emulsion, the possibility of having two bubbles coalescing to form a bigger bubble cannot be completely avoided. Besides varying the gas flow rate, one can also consider optimising the surfactant used and its concentration [35].

3.2. Loading of BSA

Two different methods can be used to load a drug in CHT microparticles. Either the drug is added to an aqueous solution of chitosan and dissolved into it prior to the particle's formation, or the drug is added in a dispersion of the already prepared particles and adsorbed on their surface. Normally, water soluble drugs are incorporated, whilst poor-water soluble drugs are adsorbed [36]. However, some drugs show specific properties that do not allow them to be incorporated in the polymers structure, since they cannot withstand some of the conditions required in the production process [37]. In other cases it is advantageous to adsorb proteins or to immobilize enzymes in the particles surface [38–41]. Because of chitosan's functional groups and thus the possibility of chemical modification, this material becomes ideal for drug adsorption [37]. Of course, in this case, there is a limitation in the amount of drug that can be loaded, which can be below the required amount to show an effect. By having a pore structure, the active surface area of the particle is increased and consequently the adsorption sites. Also, the pore volume will allow for the molecules to be entrapped in a higher concentration [12]. Because of all these possibilities of drug loading, in this work we focused on the preparation of porous chitosan microparticles using membrane emulsification process.

Besides studying the two methodologies of BSA loading, we also studied the effect of the pores on the release. In Fig. 5 we have a representation of the four formulations tested: dense_inc and porous_inc, where the BSA is encapsulated within the chitosan particles (Fig. 5A/B), and dense_ads and porous_ads, with the BSA being adsorbed to the surface (Fig. 5C/D).

In order to evaluate the drug loading in each of the formulations, the encapsulation efficiency was calculated. This information is important to understand how much of the initial BSA added to the particles actually stays within or adsorbed. In Table 1 the percentage of BSA loaded in the four formulations is shown. As expected, the formulations when the BSA was encapsulated show loadings in the range of the 93.9 ± 2.7 % and 97.6 ± 1.8 % for dense and porous particles respectively. Because the BSA is dissolved in the chitosan prior to the particle formation, when the crosslinking happens, most of the BSA is going to be entrapped within the particles' structure. The losses of around 5 % might be related to BSA that was not dissolved properly in the chitosan solution.

As for the particles with adsorbed BSA, the loading percentages are lower, which is expected since the loading area is limited to the active surface of the particles. However, there is a significant difference between the dense (40.6 ± 9.7 %) and porous particles (70.1 ± 4.3 %). Because of the existence of the porous structure, the active surface area of the particles increases. Also, the pore volume

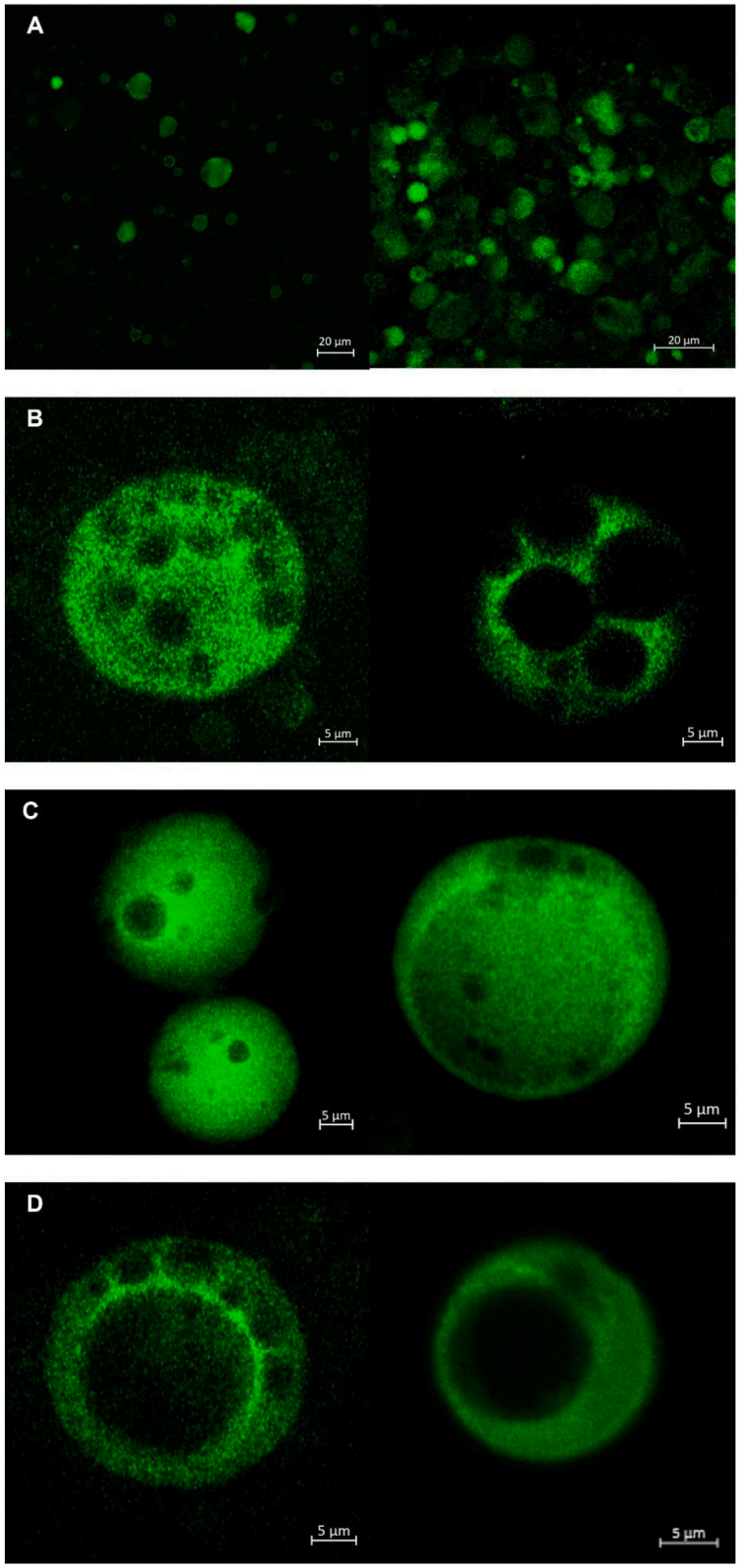

Fig. 4. Confocal microscopy images. CHT porous particles obtained using an argon flow rate of (A/B) 0.24 L h^{-1}, (C) 0.06 L h^{-1} and (D) 0.9 L h^{-1}.

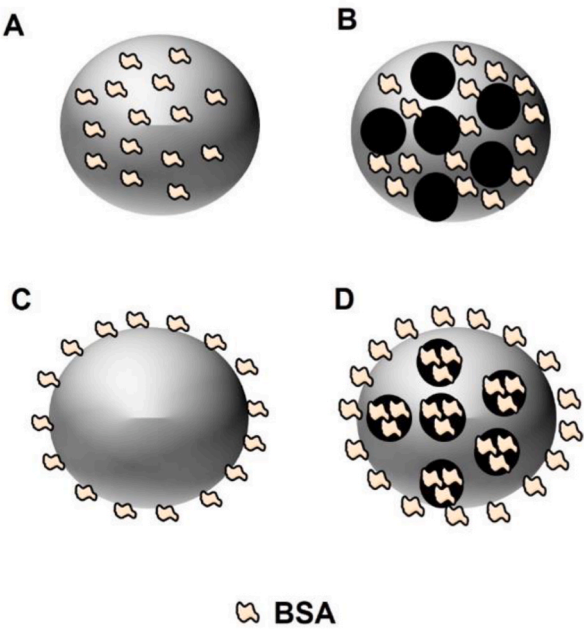

Fig. 5. Schematic representation of the four formulations prepared for the loading of BSA. The BSA as either incorporated in the structure (A/B) or adsorbed at the surface (C/D) of dense (A/C) and porous (B/D) chitosan particles.

Table 1
BSA loading efficiency for the different formulations: dense_inc (dense particles with incorporated BSA), porous_inc (porous particles with incorporated BSA), dense_ads (dense particles with adsorbed BSA) and porous_ads (porous particles with adsorbed BSA).

Formulation	Loading efficiency (%)
Dense_inc	93.9 ± 2.7 %
Porous_inc	97.6 ± 1.8 %
Dense_ads	40.6 ± 9.7 %
Porous_ads	70.1 ± 4.3 %

allows for a larger amount of BSA to stay entrapped. This shows the main advantage related to the presence of a porous structure and how the loading of drugs that cannot be processed with the particles can be increased by adding pores.

3.3. BSA release studies

The release of a drug from chitosan microparticles can happen through different mechanisms: desorption from the surface, diffusion from the swelling of the polymer, or from erosion or degradation [40,42]. For the release studies, two main components were varied: the porous structure of the particles, and the BSA loading methodology. This way, we could understand the effect of the porosity on the release profile and also to observe the differences in the release kinetics related to the main location of BSA in the particles. In Fig. 6 we have a release profile for the four experiments during (Fig. 6A) 50 and (Fig. 6B) 10 h.

In the case of dense_ads and porous_ads particles, a very similar and fast release was shown, with the total amount of BSA being released within 6 h. When loading the BSA by adsorption, the protein will form weak ionic bonds with the surface of the chitosan thus leading to its fast diffusion when in solution [43]. Due to the pH of the PBS (7.4), BSA is above its isoelectric point – 4.8 – meaning that is negatively charged and able to bond the positive charge of the chitosan chains [44]. The fact that the CHT particles have a porous structure, allows for a higher degree of diffusion, thus leading to an even faster release in the initial hours (Fig. 5B) [45]. In Fig. 5A it is possible to see that the dense_inc and porous_inc particles show the slowest release, with all of the BSA being in the solution after 24 and 48 h respectively. In this case, the BSA is encapsulated during the emulsion process, which means its diffusion to the PBS happens firstly by de-adsorption of some BSA present in the surface, but mostly by swelling of the chitosan, which forms small pores in between the polymeric chains [44]. On a later stage there might be some release related with degradation but taking into account the time it takes to release the full amount of BSA, this is less probable. In Fig. 5B it is more susceptible to see the release profile of the dense_inc particles. Initially it is not significantly different than the release of dense_ads, which can prove that the initial burst release is due to

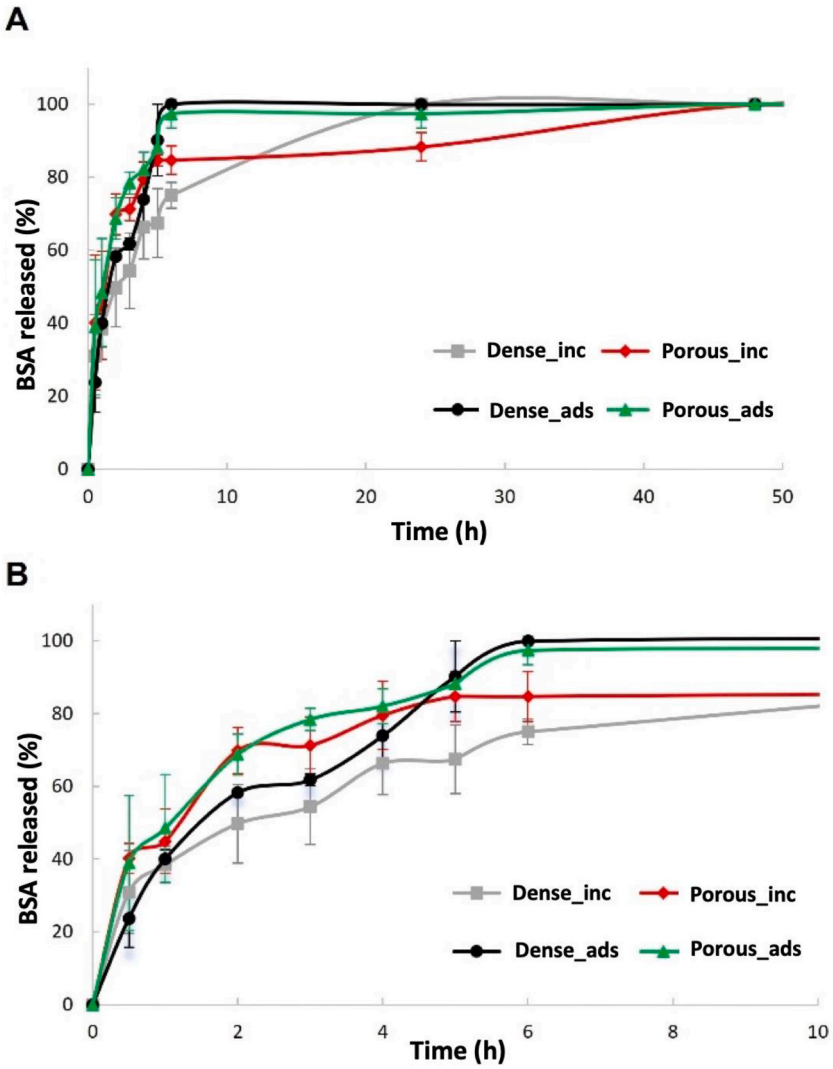

Fig. 6. Kinetic studies of the % of BSA released for 50 h (A) and for 10 h (B) for the four formulations.

the diffusion of the BSA in the surface or BSA that is located very closely to the surface of the particles. From the 5 h on, we start to see a decrease in the release rate for the dense_ads, which most likely is related to the diffusion of the BSA located in the inner part of the particles. Similarly, the porous_inc profile coincides with the release profile of the porous_ads particles until hour 6, and then the rate of release slows down. Lastly, we can also compare the dense_inc and porous_inc particles. The release is faster in the porous particles, as expected, because the higher surface area also allows for a faster diffusion of the BSA when the swelling happens. However, because the initial release related to the de-adsorption takes longer in the case of the porous particles, that leads to a delayed release related to the swelling.

Overall, the CHT particles with incorporated BSA showed a more controlled release. However, regarding the particles with adsorbed BSA, the pore structure showed to be advantageous not only in the release profile, but also in the loading.

4. Conclusions

In this work we prepared a G/W/O double emulsion using argon to produce micro-sized bubbles to entrap inside chitosan microparticles. For the first time, direct membrane emulsification technology was used to obtain porous particles, using a gas as the pore structure precursor. Track-etched membrane with 0.08 μm nominal pore size was used to formulate gas-in-chitosan solution emulsions and then they were further emulsified in a PO/PE system by use of a isoporous stainless steel membranes (9 μm pore size). Eventually the G/W/O emulsions were cross-linked to form porous particles. Thereafter a model drug was loaded in these particles by surface adsorption and also incorporating inside the particle matrix. Similar drug loading was done to the dense particles (without gas as precursor) those were produced as well. Finally, a comparative analysis of the drug release profile was studied for the four different

particles produced.

It was observed that the porous chitosan particles where drug was incorporated in the matrix had highest loading efficiency as they created more available effective surface area. Also these particles exhibited a faster release kinetics (~80 % in 6 h) in the initial hours and then slowly released 100 % in 50 h. Furthermore, it was noted that the porous structure of the chitosan particles did not affect their size and morphology. Hence the porous particles can be very promising proof-of-concept model for maximum drug loading and controlled release applications. In order to further investigate the viability of these particles as model drug carrier, certain factors like porosities, use of different biodegradable polymeric materials etc can be explored in the future.

Data availability

No data was used for the research described in the article.

CRediT authorship contribution statement

Suchintan Mondal: Formal analysis, Data curation, Investigation, Methodology, Validation, Writing – original draft. **Márcia T. Tavares:** Writing – original draft, Methodology, Data curation, Formal analysis, Investigation. **Carla Brazinha:** Writing – review & editing, Resources, Funding acquisition, Conceptualization.

Declaration of competing interest

The authors declare that they have no known competing financial interests or personal relationships that could have appeared to influence the work reported in this paper.

Acknowledgements

SM acknowledges financial support from Fundação para a Ciência e a Tecnologia (FCT), Portugal for PhD grant SFRH/BD/146967/2019.

MT acknowledges financial support from Fundação para a Ciência e a Tecnologia (FCT), Portugal for the post-doctoral contract within the "MembraneNanoDelivery" project, reference FCT 2017 02/SAICT/2017.

This research was supported by "AntiviralNADES" project (Ref. Number: 2022.08919. PTDC) funded by FCT and the Associate Laboratory for Green Chemistry - LAQV which is financed by national funds from FCT/MCTES (10.54499/LA/P/0008/2020, 10.54499/UIDP/50006/2020 and 10.54499/UIDB/50006/2020).

References

[1] S.L. Duraikkannu, R. Castro-Muñoz, A. Figoli, A review on phase-inversion technique-based polymer microsphere fabrication, Colloid Interface Sci Commun 40 (2021) 100329, https://doi.org/10.1016/J.COLCOM.2020.100329.
[2] K. Thananukul, C. Kaewsaneha, P. Opaprakasit, N. Lebaz, A. Errachid, A. Elaissari, Smart gating porous particles as new carriers for drug delivery, Adv. Drug Deliv. Rev. 174 (2021) 425–446, https://doi.org/10.1016/J.ADDR.2021.04.023.
[3] R. Parhi, Drug delivery applications of chitin and chitosan: a review, Environ. Chem. Lett. 18 (2020) 577–594, https://doi.org/10.1007/s10311-020-00963-5.
[4] S. Hassani, A. Laouini, H. Fessi, C. Charcosset, Preparation of chitosan–TPP nanoparticles using microengineered membranes – effect of parameters and encapsulation of tacrine, Colloids Surf. A Physicochem. Eng. Asp. 482 (2015) 34–43, https://doi.org/10.1016/J.COLSURFA.2015.04.006.
[5] L. Tao, J. Jiang, Y. Gao, C. Wu, Y. Liu, Biodegradable alginate-chitosan hollow nanospheres for codelivery of doxorubicin and paclitaxel for the effect of human lung cancer A549 cells, BioMed Res. Int. (2018), https://doi.org/10.1155/2018/4607945.
[6] L.Y. Wang, Y.H. Gu, Q.Z. Zhou, G.H. Ma, Y.H. Wan, Z.G. Su, Preparation and characterization of uniform-sized chitosan microspheres containing insulin by membrane emulsification and a two-step solidification process, Colloids Surf. B Biointerfaces 50 (2006) 126–135, https://doi.org/10.1016/j.colsurfb.2006.05.006.
[7] S. Mondal, B. Alke, A.M. de Castro, P. Ortiz-Albo, U.T. Syed, J.G. Crespo, C. Brazinha, Design of enzyme loaded W/O emulsions by direct membrane emulsification for CO2 capture, Membranes 12 (2022), https://doi.org/10.3390/membranes12080797.
[8] R. Berendsen, C. Güell, M. Ferrando, Spray dried double emulsions containing procyanidin-rich extracts produced by premix membrane emulsification: effect of interfacial composition, Food Chem. 178 (2015) 251–258, https://doi.org/10.1016/J.FOODCHEM.2015.01.093.
[9] P.-P. Lv, W. Wei, F.-L. Gong, Y.-L. Zhang, H.-Y. Zhao, J.-D. Lei, L.-Y. Wang, G.-H. Ma, Preparation of uniformly sized chitosan nanospheres by a premix membrane emulsification technique, Ind. Eng. Chem. Res. 48 (2009) 8819–8828, https://doi.org/10.1021/ie801758e.
[10] S. Morelli, R.G. Holdich, M.M. Dragosavac, Chitosan and Poly (Vinyl Alcohol) microparticles produced by membrane emulsification for encapsulation and pH controlled release, Chem. Eng. J. 288 (2016) 451–460, https://doi.org/10.1016/J.CEJ.2015.12.024.
[11] W. Wang, C. Luo, S. Shao, S. Zhou, Chitosan hollow nanospheres fabricated from biodegradable poly-d,l-lactide-poly(ethylene glycol) nanoparticle templates, Eur. J. Pharm. Biopharm. 76 (2010) 376–383, https://doi.org/10.1016/J.EJPB.2010.08.009.
[12] L. Qiao, L. Zhao, C. Liang, K. Du, The construction of porous chitosan microspheres with high specific surface area by using agarose as the pore-forming agent and further functionalized application in bioseparation, J. Mater. Chem. B 7 (2019) 5510–5519, https://doi.org/10.1039/C9TB01157A.
[13] Biodegradable Alginate-Chitosan Hollow Nanospheres for Codelivery of Doxorubicin and Paclitaxel for the Effect of Human Lung Cancer A549 Cells , (n.d.).
[14] T. Basu, B. Pal, S. Singh, Hollow chitosan nanocomposite as drug carrier system for controlled delivery of ramipril, Chem. Phys. Lett. 706 (2018) 465–471, https://doi.org/10.1016/J.CPLETT.2018.06.053.
[15] H. Zhang, Q. Dang, C. Liu, D. Cha, Z. Yu, W. Zhu, B. Fan, Uptake of Pb(II) and Cd(II) on chitosan microsphere surface successively grafted by methyl acrylate and diethylenetriamine, ACS Appl. Mater. Interfaces 9 (2017) 11144–11155, https://doi.org/10.1021/acsami.7b00480.
[16] J. Wan, H.A. Stone, Coated gas bubbles for the continuous synthesis of hollow inorganic particles, Langmuir 28 (2012) 37–41, https://doi.org/10.1021/la203824f.
[17] R. Chen, P.-F. Dong, J.-H. Xu, Y.-D. Wang, G.-S. Luo, Controllable microfluidic production of gas-in-oil-in-water emulsions for hollow microspheres with thin polymer shells, Lab Chip 12 (2012) 3858–3860, https://doi.org/10.1039/C2LC40387K.

[18] Y. Xia, X. Na, J. Wu, G. Ma, The horizon of the emulsion particulate strategy: engineering hollow particles for biomedical applications, Adv. Mater. 31 (2019) 1801159, https://doi.org/10.1002/adma.201801159.
[19] E. Stride, A.E. Mohan Edirisinghe, Novel preparation techniques for controlling microbubble uniformity: a comparison, (n.d.). https://doi.org/10.1007/s11517-009-0490-8.
[20] Z. Chen, J. Xu, Y. Wang, Gas-liquid-liquid multiphase flow in microfluidic systems – a review, Chem. Eng. Sci. 202 (2019) 1–14, https://doi.org/10.1016/J.CES.2019.03.016.
[21] Z. Chen, F.N. Sang, J.H. Xu, G.S. Luo, Y.D. Wang, Efficient enrichment and recovery of rare earth elements with low concentration by membrane dispersion micro-extractors, Chemical Engineering and Processing - Process Intensification 127 (2018) 127–135, https://doi.org/10.1016/J.CEP.2018.03.004.
[22] J.-H. Xu, R. Chen, Y.-D. Wang, G.-S. Luo, Controllable gas/liquid/liquid double emulsions in a dual-coaxial microfluidic device, Lab Chip 12 (2012) 2029–2036, https://doi.org/10.1039/C2LC21193A.
[23] P. Anastas, N. Eghbali, Green chemistry: principles and practice, Chem. Soc. Rev. 39 (2010) 301–312, https://doi.org/10.1039/B918763B.
[24] C.Z. Wu, Y. Xie, L.Y. Lei, S.Q. Hu, C.Z. OuYang, Synthesis of new-phased VOOH hollow "dandelions" and their application in lithium-ion batteries, Adv. Mater. 18 (2006) 1727–1732, https://doi.org/10.1002/adma.200600065.
[25] M. Kukizaki, M. Goto, Size control of nanobubbles generated from Shirasu-porous-glass (SPG) membranes, J. Membr. Sci. 281 (2006) 386–396, https://doi.org/10.1016/J.MEMSCI.2006.04.007.
[26] M. Kukizaki, Y. Baba, Effect of surfactant type on microbubble formation behavior using Shirasu porous glass (SPG) membranes, Colloids Surf. A Physicochem. Eng. Asp. 326 (2008) 129–137, https://doi.org/10.1016/J.COLSURFA.2008.05.025.
[27] R. Melich, J.P. Valour, S. Urbaniak, F. Padilla, C. Charcosset, Preparation and characterization of perfluorocarbon microbubbles using Shirasu Porous Glass (SPG) membranes, Colloids Surf. A Physicochem. Eng. Asp. 560 (2019) 233–243, https://doi.org/10.1016/J.COLSURFA.2018.09.058.
[28] Y. Chen, Z. Lu, Q. Liu, Janus membrane emulsification for facile preparation of hollow microspheres, J. Membr. Sci. 592 (2019) 117384, https://doi.org/10.1016/J.MEMSCI.2019.117384.
[29] U.T. Syed, I. Leonardo, R. Lahoz, F.B. Gaspar, R. Huertas, M.T.B. Crespo, M. Arruebo, J.G. Crespo, V. Sebastian, C. Brazinha, Microengineered membranes for sustainable production of hydrophobic deep eutectic solvent-based nanoemulsions by membrane emulsification for enhanced antimicrobial activity, ACS Sustain. Chem. Eng. 8 (2020) 16526–16536, https://doi.org/10.1021/acssuschemeng.0c05612.
[30] V. Smuleac, D.A. Butterfield, S.K. Sikdar, R.S. Varma, D. Bhattacharyya, Polythiol-functionalized alumina membranes for mercury capture, J. Membr. Sci. 251 (2005) 169–178, https://doi.org/10.1016/J.MEMSCI.2004.11.012.
[31] S. Khirani, P. Kunwapanitchakul, F. Augier, C. Guigui, P. Guiraud, G. Hébrard, Microbubble generation through porous membrane under aqueous or organic liquid shear flow, Ind. Eng. Chem. Res. 51 (2012) 1997–2009, https://doi.org/10.1021/ie200604g.
[32] M.G.A. Kassem, A.M.M. Ahmed, H.H. Abdel-Rahman, A.H.E. Moustafa, Use of Span 80 and Tween 80 for blending gasoline and alcohol in spark ignition engines, Energy Rep. 5 (2019) 221–230, https://doi.org/10.1016/J.EGYR.2019.01.009.
[33] J. Schindelin, I. Arganda-Carreras, E. Frise, V. Kaynig, M. Longair, T. Pietzsch, S. Preibisch, C. Rueden, S. Saalfeld, B. Schmid, J.-Y. Tinevez, D.J. White, V. Hartenstein, K. Eliceiri, P. Tomancak, A. Cardona, Fiji: an open-source platform for biological-image analysis, Nat. Methods 9 (2012) 676–682, https://doi.org/10.1038/nmeth.2019.
[34] Z. Toprakcioglu, T.A. Hakala, A. Levin, C.F.W. Becker, G.G.L. Bernandes, T.P.J. Knowles, Multi-scale microporous silica microcapsules from gas-in water-in oil emulsions, Soft Matter 16 (2020) 3082–3087, https://doi.org/10.1039/C9SM02274K.
[35] M. Kukizaki, M. Goto, Spontaneous formation behavior of uniform-sized microbubbles from Shirasu porous glass (SPG) membranes in the absence of water-phase flow, Colloids Surf. A Physicochem. Eng. Asp. 296 (2007) 174–181, https://doi.org/10.1016/J.COLSURFA.2006.09.042.
[36] M. Dash, F. Chiellini, R.M. Ottenbrite, E. Chiellini, Chitosan—a versatile semi-synthetic polymer in biomedical applications, Prog. Polym. Sci. 36 (2011) 981–1014, https://doi.org/10.1016/J.PROGPOLYMSCI.2011.02.001.
[37] S.M. Ahsan, M. Thomas, K.K. Reddy, S.G. Sooraparaju, A. Asthana, I. Bhatnagar, Chitosan as biomaterial in drug delivery and tissue engineering, Int. J. Biol. Macromol. 110 (2018) 97–109, https://doi.org/10.1016/J.IJBIOMAC.2017.08.140.
[38] A.L.P.F. Caroni, C.R.M. de Lima, M.R. Pereira, J.L.C. Fonseca, The kinetics of adsorption of tetracycline on chitosan particles, J. Colloid Interface Sci. 340 (2009) 182–191, https://doi.org/10.1016/J.JCIS.2009.08.016.
[39] M. Bilal, Z. Jing, Y. Zhao, H.M.N. Iqbal, Immobilization of fungal laccase on glutaraldehyde cross-linked chitosan beads and its bio-catalytic potential to degrade bisphenol A, Biocatal. Agric. Biotechnol. 19 (2019) 101174, https://doi.org/10.1016/J.BCAB.2019.101174.
[40] D. Wang, W. Jiang, Preparation of chitosan-based nanoparticles for enzyme immobilization, Int. J. Biol. Macromol. 126 (2019) 1125–1132, https://doi.org/10.1016/J.IJBIOMAC.2018.12.243.
[41] J. Kaushal, Seema, G. Singh, S.K. Arya, Immobilization of catalase onto chitosan and chitosan–bentonite complex: a comparative study, Biotechnology Reports 18 (2018), https://doi.org/10.1016/j.btre.2018.e00258.
[42] M.A. Mohammed, J.T.M. Syeda, K.M. Wasan, E.K. Wasan, Pharmaceutics an overview of chitosan nanoparticles and its application in non-parenteral, Drug Deliv. (2017), https://doi.org/10.3390/pharmaceutics9040053.
[43] P. Arnaldi, L. Pastorino, O. Monticelli, On an effective approach to improve the properties and the drug release of chitosan-based microparticles, Int. J. Biol. Macromol. 163 (2020) 393–401, https://doi.org/10.1016/J.IJBIOMAC.2020.07.016.
[44] M. Vandana, S.K. Sahoo, Optimization of physicochemical parameters influencing the fabrication of protein-loaded chitosan nanoparticles, Nanomedicine. 4 (2009) 773–785, https://doi.org/10.2217/nnm.09.54.
[45] J.M. Unagolla, A.C. Jayasuriya, Drug transport mechanisms and in vitro release kinetics of vancomycin encapsulated chitosan-alginate polyelectrolyte microparticles as a controlled drug delivery system, Eur. J. Pharmaceut. Sci. 114 (2018) 199–209, https://doi.org/10.1016/J.EJPS.2017.12.012.